HHS Public Access

Author manuscript

J Mol Biol. Author manuscript; available in PMC 2017 June 22.

Published in final edited form as:

J Mol Biol. 2017 January 20; 429(2): 192–207. doi:10.1016/j.jmb.2016.12.012.

The C-Box Region of MAF1 Regulates Transcriptional Activity and Protein Stability

Ajay Pradhan[1], **Amy M. Hammerquist**[1,2], **Akshat Khanna**[1,2], and **Sean P. Curran**[1,2]

[1]Leonard Davis School of Gerontology, University of Southern California, Los Angeles, CA 90089, USA

[2]Department of Molecular and Computational Biology, Dornsife College of Letters, Arts, and Sciences, University of Southern California, Los Angeles, CA 90089, USA

Abstract

MAF1 is a conserved negative regulator of RNA polymerase (pol) III and intracellular lipid homeostasis across species. Here, we show that the MAF1 C-box region negatively regulates its activity. Mutations in *Caenorhabditis elegans mafr-1* that truncate the C-box retain the ability to inhibit the transcription of RNA pol III targets, reduce lipid biogenesis, and lower reproductive output. In human cells, C-box deletion of MAF1 leads to increased MAF1 nuclear localization and enhanced repression of *ACC1* and *FASN,* but with impaired repression of RNA pol III targets. Surprisingly, C-box mutations render MAF1 insensitive to rapamycin, further defining a regulatory role for this region. Two MAF1 species, $MAF1_L$ and $MAF1_S$, are regulated by the C-box YSY motif, which, when mutated, alters species stoichiometry and proteasome-dependent turnover of nuclear MAF1. Our results reveal a role for the C-box region as a critical determinant of MAF1 stability, activity, and response to cellular stress.

Keywords

MAF1; RNA polymerase III; lipid metabolism; *Caenorhabditis elegans*; mTOR

Introduction

RNA polymerases (pol) I, II, and III catalyze DNA-dependent RNA synthesis that is required for the regulation of protein biogenesis and maintenance of cellular homeostasis. RNA pol III is responsible for the synthesis of 5S rRNA, U6 snRNA, and tRNAs, and its regulation is essential for proper cell growth and survival during stress [37,40]. In yeast, Maf1 is a global repressor of RNA pol III that is involved in cellular stress responses, including nutrient starvation, DNA damage, and exposure to cytotoxic drugs [4,35,40]. Additionally, in the unstressed state, Maf1 translocation to the nucleus and subsequently

Correspondence to Sean P. Curran: Leonard Davis School of Gerontology, University of Southern California, Los Angeles, CA 90089, USA. spcurran@usc.edu.

Supplementary data to this article can be found online at http://dx.doi.org/10.1016/j.jmb.2016.12.012.

Author contributions: Conceptualization, S.P.C.; Methodology, A.P., A.M.H., A.K., and S.P.C.; Investigation, A.P., A.M.H., A.K., and S.P.C.; Writing, A.P. and S.P.C.; Supervision, Project Administration, and Funding Acquisition, S.P.C.

RNA pol III repression is prevented by phosphorylation, while loss of phosphorylation leads to Maf1 accumulation in the nucleus [20,26,39].

In yeast, target of rapamycin (TOR) complex 1 (TORC1) has been implicated as a key determinant of Maf1 regulation that affects Maf1 localization and function. Protein phosphatase 2A, protein kinase A (PKA), and Sch9 are components of the TOR pathway that modify the phosphorylation of Maf1 to influence its function [2,20]. Mutations of PKA phosphorylation sites in yeast Maf1 result in nuclear accumulation without affecting pol III activity [19]. This suggests that the coordination of Maf1 dephosphorylation, nuclear accumulation, and negative regulation of RNA pol III transcription can be uncoupled and that there could be other unknown factors that regulate Maf1. Different post-translational modifications of human MAF1 also impact cellular localization and activity. Human MAF1 has at least three TORC1 phosphorylation sites (S60/68/75) that regulate nuclear localization and function. In addition to phosphorylation, SUMOylation also impacts human MAF1 activity, without changing MAF1 localization [27], indicating that there are multiple levels of MAF1 regulation at play [28].

Maf1 has been shown to impact several physiological functions. Maf1 can negatively regulate lipid homeostasis [10,22] and reproduction [1,10]. The ability of Maf1 to regulate intracellular lipids is tied to the repression of *de novo* fatty acid biosynthesis, specifically by its recruitment to the *FASN* promoter and inhibition of sterol regulatory element binding protein 1 (SREBP1)-mediated transcription [22]. Moreover, Maf1 is also downregulated in different primary human liver cancer cells [13,22].

The Maf1 protein has been characterized to contain three conserved regions named the A-, B-, and C-box. The A-box and B-box regions are known to form a complex with RNA pol III large subunits and Brf1, respectively [24], while the role of the C-box is largely unknown. In order to define the function of the C-box region, we used a *Caenorhabditis elegans* strain harboring a *mafr-1(tm6082)* mutation that leads to a deletion of the C-box and to a human MAF1 construct with a deleted C-box. Here, we report that the C-box region alters the abundance of two distinct species of human MAF1. In worms, C-box mutations in MAF1 result in hyperactive repression of target genes and impact other physiological processes, including reproduction and lipid homeostasis. In human cell culture, we define the YSY motif in the C-box as critical for MAF1 stability and regulation. The results of this study identify a new mechanism by which Maf1 is regulated to differentially impact multiple aspects of gene regulation and cell biology.

Results

Mutations that truncate the C-box of *C. elegans* MAFR-1 lead to gain-of-function phenotypes

We previously reported that overexpression of *C. elegans* MAFR-1 reduced organismal lipid storage and fecundity (Fig. 1A), in addition to its previously established role in negatively regulating RNA pol III [10]. In this study, we explored the regulatory role of the C-box region of MAF1 in both *C. elegans* and human cell culture. In order to understand the role of the C-box, we utilized a deletion allele, *tm6082*, of *C. elegans mafr-1*, which removes the

entire C-box region and modifies the C-terminal end of the protein due to a frameshift mutation (Fig. 1B and S1A). To assess the impact of this mutation on MAFR-1-sensitive transcriptional targets, we performed a microarray analysis comparing *mafr-1(tm6082)* mutants to animals overexpressing *mafr-1*. Surprisingly, we found that *mafr-1(tm6082)* mutants display a gene expression profile similar to animals overexpressing *mafr-1* that have enhanced MAFR-1-dependent repression of RNA pol III targets [10]. Specifically, of the 1503 genes downregulated in *mafr-1(tm6082)* animals, 872 of these genes were also downregulated (from a pool of 900 downregulated genes) in a strain with a single additional copy of *mafr-1* expressed (Fig. 1C). This indicates that the *mafr-1(tm6082)* mutation is hyperactive compared to the wild-type (WT) MAFR-1. Gene ontology (GO) term category analysis of *mafr-1(tm6082)* animals was enriched for genes involved in cellular organization, development, and reproduction processes (Fig. 1D). Specifically, despite the loss of the C-box region, *mafr-1(tm6082)* animals display enhanced negative regulation of RNA pol III genes, including pre-initiator methionine, methionine, and Tyr (GTA) tRNAs (Fig. 1E), and also RNA pol II genes, including components of the RNA pol III transcription factor, TFIIIB complex, *tbp-1* and *brf-1* (Fig. 1F and G).

We next assessed the organism-level impact of the *mafr-1(tm6082)* mutation and noted additional phenotypic similarities we previously reported in the single copy *mafr-1*o/e strain [10], which further support a gain-of-function nature of the *tm6082* allele. Specifically, we documented a 24% reduction in stored intracellular lipids as compared to WT animals, without altering body size (Fig. 2A and B and S1B and C). Importantly, *mafr-1* RNA interference (RNAi) treatment rescued the reduced fat phenotype in *mafr-1(tm6082*) animals, which not only reveals that the phenotype was dependent on MAFR-1 but also supports the gain-of-function nature of the allele. Previous studies in both *C. elegans* and mammals have indicated that the intracellular lipid phenotype is mediated, at least, in part, through MAF1 regulation of *de novo* lipid biogenesis genes [10,22]. In support of these previous studies, *mafr-1(tm6082)* animals have significant reduction in the expression of both *fasn-1/FASN* and *pod-2/ACC1* (Fig. 2C and D).

Similarly, fecundity was also reduced in *mafr-1(tm6082)* animals with diminished reproductive output from day 2 of adulthood, which continually declined until day 4 (reproductive senescence; Fig. 2E) that resulted in an overall reduction in total brood size, which is similar to animals overexpressing *mafr-1* (Fig. S1D). MAFR-1-mediated loss of fecundity was previously correlated with a reduction in the expression of the vitellogenin family of genes [10], which are key mediators of lipid transport to developing oocytes [12]. We measured a significant reduction in the four major *vit* genes in *mafr-1(tm6082)* animals (Fig. 2F) that was also detectable in our microarray analysis (Table S1). The loss of vitellogenesis is likely a contributing factor to the overall decline in reproduction in *mafr-1(tm6082)* animals and may contribute to the deregulation of reproduction genes (Fig. 1D) [7,15,31].

Because we had previously demonstrated that *C. elegans* MAFR-1 could regulate mammalian MAF1 targets, we expressed a C-terminal green fluorescence protein (GFP) or C-terminal 3X-Flag-tagged version of *mafr-1(tm6082)* in HEK-293T cells and discovered that the resulting truncation of C-box resulted in greater nuclear accumulation of the protein

as compared to the WT protein (Fig. 2G and S2A). Cloning of the unique 37 aa at the C-terminal end of *mafr-1(tm6082)* revealed that this sequence is sufficient to drive monomeric GFP localization to the nucleus, which suggests that this novel sequence contains an nuclear localization signal (NLS)-like motif (Fig. S2B). Quantitative real time PCR(qRT-PCR) analysis of total RNA isolated from HEK-293T cells expressing either *mafr-1* or *mafr-1(tm6082)* reveals that either proteins lead to a significant downregulation of RNA pol III target genes, including pre-tRNA^{Leu} and U6 snRNA and RNA pol II targets, *FASN* and *ACC1* (Fig. 2H). Despite lower total protein levels (Fig. 2G), the truncated version of MAFR-1 is a more potent inhibitor of MAF1 target gene transcription than the WT protein (Fig. 2H), which is consistent with the notion that this is a gain-of-function mutation.

The C-box region regulates the stoichiometry of two hMAF1 species

In light of our findings that *C. elegans* MAFR-1 and human MAF1 share common functions [10], we next examined the role of the C-box region in human MAF1 by deleting this region (ΔC), but without the addition of the NLS-like sequence in *mafr-1(tm6082)*, which could impact activity (Fig. 3A). We noted that, when resolved by 2-(*N*-morpholino)ethanesulfonic acid (MES)buffered SDS-PAGE, WT MAF1 migrates as two distinct bands, with the abundance of the larger ($MAF1_L$) species being dominant over the smaller ($MAF1_S$) species (Fig. 3B and C). Both proteins are reduced in cells treated with MAF1 siRNA (Fig. 3D), which indicates they are both MAF1 polypeptides. Intriguingly, two species also exist for the mutated ΔC protein; however, the ratio of these two species of MAF1 is flipped, such that the ΔC_S species is more abundant than ΔC_L (Fig. 3B and C). The identification of two species of MAF1, even when the C-box is removed, suggests that the smaller MAF1 species is not a result of modification to the C-terminal end of the protein. The large and small species of MAF1 and ΔC are more abundant in the cytoplasm, and the deletion of the C-box (ΔC) resulted in an increase in the nuclear accumulation of the ΔC_S protein as compared to the WT protein (Fig. 3B and C).

The relationship between the large and small species of MAF1 is not known. However, our ability to distinguish each of them by gel electrophoresis, despite not knowing the basis of the differential mobility, affords the means to biochemically characterize their individual responses to molecular manipulation *en masse*. Previous studies have observed multiple MAF1 bands, which are often dismissed as probable phosphorylated forms of MAF1. However, phosphatase treatment does not abolish either species (Fig. 3E). We similarly investigated whether the *C. elegans* MAFR-1 protein exists in multiple forms but could not clearly resolve a species with electrophoretic mobility different from that of the major form of MAFR-1 (Fig. S2C and D). However, we did note that when MAFR-1 is expressed in HEK-293T cells that are treated with the proteasome inhibitor peptide MG-132, a faster migrating species is stabilized (Fig. 2G).

The C-box region regulates nuclear MAF1 stability by the ubiquitin proteasome system (UPS)

The mechanisms that regulate MAF1 turnover are not understood. Our examination of the *C. elegans* MAFR-1 protein identified reduced abundance but enhanced the activity of the MAFR-1(tm6082) protein as compared to WT MAFR-1 (Fig. 2H). This begged the question

of how MAF1 protein levels are maintained. The UPS represents one major pathway to maintain cellular proteostasis. To test a role for the UPS in MAFR-1 regulation, we treated HEK-293T cells expressing *mafr-1* or *mafr-1(tm6082)* with the proteasome inhibitor peptide MG-132, fractionated proteins from the nuclear and cytoplasmic compartments, and measured MAFR-1 abundance. Surprisingly, cytoplasmic MAFR-1 abundance was not altered by MG-132 treatment, while nuclear MAFR-1 protein was clearly enriched (Fig. 2G). This finding suggests that nuclear MAFR-1 is targeted for degradation by the UPS. Notably, the *tm6082* mutant form of MAFR-1 was less sensitive to MG-132 treatment, suggesting that the C-box region plays an important role in MAFR-1 proteostasis.

We next treated cells expressing WT or ΔC versions of MAF1 with MG-132 and examined protein stability. Compellingly, $MAF1_L$ was largely unaffected by MG-132, while $MAF1_S$ levels were increased, indicating that the small species of MAF1 is indeed turned over by the UPS (Fig. 3F and G). Both species of ΔC are stabilized by MG-132 treatment and, in light of its enhanced nuclear localization, predict that MAF1 protein turnover would occur in the nucleus, which is similar to our observations of the *C. elegans* MAFR-1 protein (Fig. 2G).

To further test the hypothesis that MAF1 turnover occurs in the nucleus, we inserted an SV40-NLS sequence at the C terminus of our MAF1 constructs, which increased MAF1:GFP nuclear localization (Fig. 3H). Similarly, biochemical fraction of cells expressing a 3X-FLAG epitope-tagged version of the MAF1-SV40-NLS protein revealed that MAF1 abundance is reduced when forced into the nucleus. Introduction of the C-terminal SV40-NLS sequence in our ΔC construct did not affect ΔC_L levels but reduced ΔC_S abundance (Fig. 3I and J and S3A). Because MG-132 targets several components of the cellular proteostasis system, including the nuclear calpains [34], we next examined the effect of a calpain-specific inhibitor PD150606 (PD) on MAF1 stability. PD150606-treated cells did not show changes in MAF1 abundance (Fig. 3I and S3B and C), which suggests that nuclear calpains do not play a significant role in MAF1 degradation. Taken together, these data support a model where the nuclear fraction of MAF1 is sensitive to the UPS for protein turnover (Fig. 3K).

The C-box region is required for rapamycin sensitivity

We identified multiple phosphorylated species of MAF1 and ΔC (Fig. 4A and B), which, as previously shown in both yeast and mammalian cells, correlate with the cytoplasmic/nuclear localization of the protein (Fig. 4C and D) [2,17,19,32]. Based on PhosTag® gel electrophoresis, ΔC is predominantly unphosphorylated, but a monophosphorylated species is also detectable (Fig. 4A and B). Starvation and rapamycin treatment have been shown to inhibit the TORC1, which leads to the loss of MAF1 phosphorylation [17]. We analyzed human cells subjected to serum starvation or treatment with either rapamycin or methyl methanesulfonate (MMS), all of which led to MAF1 dephosphorylation (Fig. 4A and B and S4A). To define the unphosphorylated species of MAF1, we treated protein samples with phosphatase and identified the fastest migrating species (labeled band #0). With this unphosphorylated species of MAF1 identified, the slower migrating bands represent the single (labeled band #1) and double (labeled band #2) phosphorylated versions of MAF1 (Fig. 4A). MMS and rapamycin treatment of cells both led to the loss of the doubly

phosphorylated species; however, 5-h growth in serum-free medium was ineffective at significantly altering MAF1 phosphorylation (Fig. 4A and B and S4A). MMS treatment resulted in a stronger dephosphorylation effect compared to rapamycin, leading to loss of both phosphorylated species (Fig. 4A and B). Unlike the WT MAF1 protein, MMS and rapamycin treatment resulted in no significant change in ΔC phosphorylation state (Fig. 4A and B), which indicates that the C-box region is important for MAF1 phosphorylation. The same results were observed with MAF1-GFP overexpression in HEK293T cells, which show increased nuclear localization of MAF1 following treatment with MMS and rapamycin (Fig. S6B).

Western blot analysis of nuclear and cytoplasmic fractions showed that rapamycin treatment increased the nuclear accumulation of $MAF1_L$, but not $MAF1_S$ (Fig. 4C and D). In contrast, the nuclear fraction of ΔC_S was reduced with rapamycin treatment (Fig. 4C and E). The rapamycin-mediated loss of nuclear ΔC_S was blocked by MG-132 treatment, with levels comparable to cells treated with MG-132 alone (Fig. 4F–H and S4B). Again, we noted the MG-132-dependent restoration of only $MAF1_S$, and nuclear/cytoplasmic fractionation revealed a stronger effect of the UPS in the nuclear fraction for $MAF1_S$ and ΔC_S as compared to the cytoplasmic fraction (Fig. 4G and H). In order to assess the temporal requirement for the combinatorial effect of rapamycin and MG-132, we varied the duration and sequence of exposure to both compounds in HEK-293T cells. Analysis of MAF1 nuclear fractions did not reveal any difference in the relative amounts of MAF1 between the treatment conditions (Fig. S4C), which, when taken together, suggests a new model for MAF1 regulation, in which rapamycin increases MAF1 nuclear localization and subsequently leads to MAF1 protein turnover by the UPS. These results reveal an important distinction in the species-specific phosphorylation and protein turnover in response to cellular stress.

Rapamycin has been shown to lead to small but measurable increases in MAF1 nuclear localization (Fig. 4C and D), which is thought to correspond to enhanced repression of MAF1-sensitive RNA pol III targets [9,16,33]. We next assessed the impact of the MAF1 C-box on the rapamycin-dependent regulation of MAF1 activity, specifically the capacity to repress the expression of RNA pol II and RNA pol III targets that are known to be sensitive to MAF1 levels. Indeed, the overexpression of MAF1 reduced the transcript levels of *pre-tRNA Leu* (Fig. 4I), *FASN* (Fig. 4J), and *ACC1* (Fig. 4K), and importantly, these targets were further reduced with rapamycin treatment. In support of our findings that the ΔC mutant is rapamycin-resistant, rapamycin treatment did not further repress these targets in cells expressing ΔC. It is notable that the ability of ΔC to repress RNA pol III targets was attenuated, but its ability to inhibit *FASN* and *ACC1* was often enhanced. Taken together, these findings define the C-box region of MAF1 as critical for MAF1 stability, responsiveness to rapamycin, and target selection.

Loss of the C-box does not impair MAF1-mediated regulation of lipid homeostasis

The increased nuclear localization of the ΔC protein, in combination with its enhanced repression of genes critical for *de novo* lipid biogenesis, led us to hypothesize that the expression of ΔC would regulate intracellular lipid levels. Because HEK-293T cells are not

ideal for metabolism studies, we expressed MAF1 or ΔC in HepG2 cells and assessed the expression of MAF1-sensitive target genes (Fig. 5A–C). Similar to HEK-293T cells, expression of either MAF1 or ΔC effectively down-regulates *FASN* and *ACC1* transcript levels (Fig. 5B and C), and expression of ΔC resulted in stronger transcriptional repression of these target genes. It is notable that the ability of ΔC to repress RNA pol III targets was significantly impaired in HepG2 cells (Fig. 5A). We next examined intracellular lipids by Oil Red O staining of cells following the expression of MAF1 or ΔC. Similar to our studies in *C. elegans,* expression of either MAF1 or ΔC in HepG2 cells resulted in a twofold reduction in total lipid droplets (Fig. 5D, E, and S5). The ΔC mutant retained its capacity to reduce intracellular lipids, which suggests that the C-box of MAF1 is not required for its cellular roles in lipid metabolism. Moreover, the enhanced repression of RNA pol II-mediated genes suggests that the C-box might even be repressive for this aspect of MAF1 activity. Taken together, these studies reveal distinct roles for the C-box region in MAF1-sensitive phenotypes.

The YSY motif in the C-box regulates MAF1 stability

The C-box region of MAF1 is defined as 53 aa in length and corresponds to 4 β-sheets in the MAF1 structure [24]. As the deletion of the C-box region leads to several gain-of-function phenotypes, we sought to identify the specific residues in the C-box that were responsible for MAF1 stability, subcellular localization, $MAF1_L/MAF1_S$ stoichiometry, and sensitivity to rapamycin. To this end, we first systematically deleted portions of the C-box, one at a time, and tested for MAF1 phosphorylation, localization, and rapamycin responsiveness (Fig. 6A). We could not detect a doubly phosphorylated species in sub-deletion 1, similar to our initial observations in the ΔC mutant (Fig. S6A). Furthermore, sub-deletions 1 and 2 mutant proteins did not respond to treatment with rapamycin (Fig. S6B). Finally, sub-deletion 2 resulted in altered stoichiometry of the large and small species with increased nuclear localization (Fig. S6C). In contrast, sub-deletion 3 (aa 190–206) was still responsive to rapamycin, albeit attenuated, which indicates that the rapamycin-sensitive region is within sub-deletion 1 (aa 150–169) and possibly sub-deletion 2 (aa 170–189; Fig. S6B). To narrow down the critical region further, we subsequently generated sub-deletion 4 (aa 160–179) and sub-deletion 5 (aa 164–169), which contain the boundary between sub-deletion 1 and 2 (Fig. 6A). Both of these constructs render MAF1 unresponsive to rapamycin (Fig. S7A,B).

Finally, to identify the specific amino acids in this region that were causal for the insensitivity to rapamycin treatment, we mutated conserved residues in this region (Fig. 6A) and observed that the $Y^{166}S^{167}Y^{168}$ motif in the C-box results in the destabilization of the $MAF1_L$ protein (Fig. 6B and S8A), which is not a result of reduced levels of transcription (Fig. S8B). Mutation of any of these residues renders MAF1 unresponsive to rapamycin as evidenced by the lack of increased nuclear accumulation (Fig. S9A) and lack of change in species migration by phos-tag gel electrophoresis (Fig. 6C and S9B and C). Similar to the ΔC construct, deletion of the entire YSY motif could possibly compromise MAF1 protein stability (Fig. 6B and S8A). However, when modeled on the MAF1 structure, this is unlikely to cause severe misfolding (Fig. S10) [30]. Moreover, single amino acid substitutions that mimic phosphorylation (Y166E, S167D, and Y168E) or complex substitution of two or more residues in the YSY motif (EAE and ESE) result in a distribution of MAF1 species

similar in migration and abundance to those observed in the ΔC mutant (Fig. S8A). Importantly, substitution of S167A in this motif is not predicted to severely compromise protein stability (Fig. S10) and, importantly, maintains a $MAF1_L/MAF1_s$ protein ratio similar to that observed in WT (Fig. 6B and S8A).

Next, we examined the functionality of the single amino acid mutations on the transcription of MAF1-senstive targets. Similar to our findings for ΔC, single amino acid substitutions that reversed the $MAF1_L/MAF1_s$ species ratio also impacted MAF1-sensitive transcriptional targets (Fig. S11). Several of these mutations that resulted in an increase in the abundance of $MAF1_s$ species displayed enhanced *FASN* and *ACC1* repression with the repression of RNA pol III targets either attenuated or unaffected. Taken together, these findings identify the differential regulation of MAF1-dependent transcripts depending on the stoichiometry of the large and small species of MAF1.

Lastly, we investigated the possible impact of the TORC1-responsive amino acids to the changes in $MAF1_L/MAF1_s$ ratio. We mutated the S68 and S75 residues of MAF1, whose phosphorylation states are most sensitive to rapamycin [16,17], but did not observe a change in MAF1 stability (Fig. S12). This indicates that the C-box region is indeed an important regulator of MAF1 stability and function independent of the well-studied TORC1-responsive domain. Moreover, altering these TORC1-sensitive residues could not restore $MAF1_L/MAF1_s$ stoichiometry when S167 is mutated (Fig. S12), supporting the gain-of-function nature when disrupting the C-box region. Together, these results suggest that the amino acids $Y^{166}S^{167}Y^{168}$ are the key residues in the C-box region that drive MAF1 stability and activity.

MAF1 is a critical component of cellular growth, adaptation, and physiology, but studies of MAF1 protein homeostasis are incomplete (Fig. 7). We find that the loss of the C-box region of MAF1 alters MAF1 localization, stability, and target selection. Moreover, we define the existence and importance of the stoichiometric ratio of $MAF1_L/MAF1_s$ species, which differentially impact cellular lipid metabolism and RNA pol III-mediated transcription. Our study uncovers new layers of MAF1 regulation, which may explain the recent contradictory findings of the physiological roles of MAF1 [1,10,22].

Discussion

Our work reveals three novel aspects of MAF1 regulation and activity. First, we define a role for the uncharacterized C-box region of MAF1, which regulates MAF1 sensitivity to rapamycin, subcellular localization, and activity as a transcriptional repressor. Second, we provide evidence that the turnover of MAF1 is regulated by the UPS, primarily when MAF1 localization is nuclear. Third, we uncover the existence of large and small species of MAF1 that are present when overexpressed in human cell lines and whose stability is influenced by the C-box. Taken together, these data define a new paradigm for how MAF1 activity is coordinated and perhaps explains the variable effects of MAF1 on animal physiology [1,22].

Our initial studies in *C. elegans* revealed a potent impact of the *mafr-1(tm6082)* mutation on organism lipid homeostasis. The underlying mechanism for MAF1 recruitment, in any

organism, to chromatin is unknown, even more so for non-RNA pol III loci. Several models agree that MAF1 can interact with either RNA pol III itself or transcription factors to prevent transcription [5,6,10,11,16,17,24,27,28]. The expressions of *pod-2/ACC1* and *fasn-1/FASN* are regulated by RNA pol II and SREBPs in *C. elegans* and mammals. We examined the expression of *C. elegans sbp-1* and other transcripts, beyond *pod-2* and *fasn-1,* which are sensitive to *sbp-1* expression. However, unlike *pod-2* and *fasn-1*, we could not detect a consistent change in expression between WT and *mafr-1(tm6082)* animals (Fig. S13) [36]. In mammals, MAF1-dependent changes in *FASN* and *ACC1* were not a result of changes in SREBP occupancy at these promoters [22], which suggests a SREBP-independent response. Moreover, our previous work identified several cell-non-autonomous roles for MAFR-1 [10]. As such, it remains possible that SBP-1 could play a role in mediating *mafr-1* phenotypes in specific tissues, but these effects are masked in our whole-animal assessment of steady-state transcript levels. The identification of MAF1 interacting proteins and mechanisms of chromatin association remains critically important.

Earlier studies of MAF1 indicated that the A-box region can form a complex with RNA pol III large subunits, while Brf1 appears to associate with Maf1 through both A- and B-box regions. [24]. However, the role that the C-box plays in Maf1 function had not previously been explored. Our results demonstrate that the C-box region plays a crucial role in regulating MAF1 stability and activity. Specifically, mutation of the C-box region resulted in enhanced nuclear localization of MAF1, hyper-repression of certain MAF1 target genes, altered $MAF1_L$ and $MAF1_S$ ratios, and insensitivity to rapamycin. Importantly, it is important to note that $MAF1_s$ is not ΔC, as mutation of the C-box region, including complete deletion, results in small and large species that migrate as distinct species in MES-buffered SDS-PAGE. Taken together, these findings describe novel functions for this conserved and critically important region in MAF1.

While our study was under review, Cai and Wei tested the *tm6082* mutant as a loss-of-function model of MAFR-1 and documented differential stress responses in *Saccharomyces cerevisiae* and *C. elegans* lacking MAF1 [3]. Our observation that animals harboring the *tm6082* allele of *mafr-1* behave similarly to animals overexpressing MAFR-1 explains the opposing phenotypes observed in yeast (loss-of-function deletion) and worms (gain-of-function truncation). Our transcriptional profiling of these two strains reveals that the *tm6082* mutation results in the downregulation of several additional genes, one of which is the initiator, and mature $tRNA^{Met}$ transcripts. Initiator $tRNA^{Met}$ has been suggested to be a limiting factor in protein synthesis [25], and the low level of $tRNA^{Met}$ could explain some of the enhanced physiological effects observed in the *tm6082* mutant animals. Collectively, our phenotypic analysis of the *tm6082* mutant as a gain-of-function mutation reveals that the phenotypes of this mutant are consistent with the loss-of-function phenotypes in yeast [3].

Our studies identify two distinct species of human MAF1 when MAF1 is expressed in human cells, which we call $MAF1_L$ and $MAF1_S$, are separated by MES-buffered SDS-PAGE. These two species have varied sensitivity to the UPS, distinct subcellular localization, and differential responses to cellular stress. Although we were unable to clearly resolve multiple species of MAFR-1 in *C. elegans*, their existence remains a possibility (Fig. S2C and D) that may be revealed as worm biochemical methodologies become more

sophisticated. It has been reported that MAF1 functions are variant among different tissues and cell types [1,10,25], and a survey of previous studies that biochemically analyzed MAF1 in different cell types reveals that the presence, abundance, and number of MAF1 species that is also variable [8,22,29,32]. We predict that these stoichiometric differences in MAF1 species might be important for the differential impact MAF1 plays on animal physiology in a cell type-dependent manner.

Apart from its canonical role in RNA pol III inhibition, Palian *et al.* and Khanna *et al.* discovered a non-canonical role of MAF1 in the negative regulation of lipid biogenesis [10,22]. Since these early studies, subsequent work in yeast has revealed that loss of Maf1 shows enlarged lipid droplets and was correlated to increased pyruvate kinase activity [18]. Moreover, a tumor suppressor function has been assigned to MAF1 [13,22], which could result from MAF1-dependent effects on lipid biosynthesis and/or RNA pol III transcription. We document reduced lipid levels in HepG2 hepatocarcinoma cells following the overexpression of human MAF1 and the C-box deleted (ΔC) construct. While the capacity of ΔC to regulate RNA pol III transcripts was attenuated, inhibition of *FASN* and *ACC1* transcripts was enhanced. This suggests that the effects of MAF1 on intracellular lipids can perhaps be uncoupled from its roles in RNA pol III. It is notable that whole body and lifelong knockout of MAF1 in mice caused the animals to develop a lean phenotype with increased protection to diet-induced obesity. Although lipogenesis was increased in the liver, the high mobilization of hepatocellular lipids *via* autophagy and/or metabolic inefficiency due to the high transcription rate of RNA pol III protected the animals from lipid accumulation [1]. In addition to the possible temporal and tissue-specific effects, these apparent opposing findings in the knockout MAF1 mice as compared to that observed in other studies and organisms could be a result of differential expression of $MAF1_L$ and $MAF1_S$, the stoichiometry of which is reversed in the ΔC mutant.

Our studies reveal that $MAF1_L$ is regulated by the TORC1 complex and is stabilized by the YSY motif in the C-box region. This larger species of MAF1 regulates all MAF1-sensitive transcripts defined so far. In contrast, ΔC protein is more nuclear, is insensitive to rapamycin, and retains its ability to regulate *FASN*, *ACC1*, and intracellular lipid abundance. The impaired ability of ΔC to regulate RNA pol III-dependent target genes while still maintaining the regulation of RNA pol II targets further supports the idea that the canonical role of MAF1 in RNA pol III inhibition and its newly described role in lipid biogenesis can be uncoupled. The negative impact on lipid biogenesis in worms following the overexpression of MAFR-1 or the presence of the *tm6082* gain-of-function allele could be due to the inhibition of RNA pol II genes including *fasn-1* and *pod-2,* whose protein products are known to carry out rate-limiting steps in lipid synthesis. Reproductive output is also reduced in both MAFR-1-overexpressed and the *tm6082* strains, possibly through the negative regulation of genes involved in reproduction, as evident from microarray analysis and qPCR analysis of vitellogenin genes. Khanna *et al.* demonstrate that the downregulation of vitellogenin genes by MAFR-1 overexpression is responsible for impacting fecundity in a cell-non-autonomous manner [10]. In contrast, Maf1 null mice showed reduction in litter size compared to the control groups [1]. Aside from the methodological differences between these studies and the likely tissue-specific differences in MAF1 function, our studies suggest that the abundance of $MAF1_L$ and $MAF1_S$ are of physiological significance. Based on our

findings, we would predict that endogenous $MAF1_S$ is rapidly turned over by the UPS. Correspondingly, it has been proven to be difficult to detect by commercially available antisera; however, its existence is notable in other studies [21]. Nevertheless, our studies suggest that it is prudent to take a second look at previous studies that have utilized overexpression in human cell lines.

Little is known with regard to the mechanisms that maintain MAF1 protein abundance. Mutation of specific residues in the C-box in MAF1 increased protein turnover *via* the proteasomal degradation pathway, which, based on our biochemical fractionation, occurs predominantly in the nucleus and with stronger effects on $MAF1_S$. This discovery is in line with other reports where PKA and Sch9 mutation in yeast leads to Maf1 nuclear accumulation and consequently lowers Maf1 abundance [2,38]. The decreased protein stability in ΔC suggests that this region also helps MAF1 to avoid being recognized by the proteasomal system. Although the deletion of the entire C-box could induce structural changes that abolish function, the MAF1-dependent phenotypes we measure are enhanced, particularly in worms, and suggest a gain-of-function phenotype. Nevertheless, our single amino acid substitutions of the YSY motif and Ser167 alone are unlikely to change the structure, based on modeling (Fig. S10), and result in similar changes in MAF1 abundance, species stoichiometry, and transcriptional target selection (Fig. S10) [30]. Taken together, our findings expand upon the established roles that phosphorylation play on the MAF1 pathway and suggest new models for regulating MAF1 function.

Collectively, we define a critical and distinct role for the MAF1 C-box in regulating MAF1 localization, stability, and function. In assessing the specific contributions that $MAF1_L$ and $MAF1_S$ play in previously documented phenotypes and molecular functions that are MAF1-dependent, we find that these two species of MAF1 are differentially regulated by TORC1, the proteasome, and confer a differential impact on target specificity. Future studies will be needed to determine whether $MAF1_S$ is derived from $MAF1_L$ or if it is synthesized *de novo*. Regardless of the mechanism of synthesis, our studies delineate a new layer of complexity while providing new mechanistic insight to MAF1 functions in cell biology.

Experimental Procedures

C. elegans growth conditions

Worms were maintained on 6-cm growth media plates supplemented with streptomycin seeded with *Escherichia coli* OP50-1 strain. For RNAi experiments, the OP50 RNAi strain [14] expressing double-stranded RNAi was seeded onto growth media plates supplemented with 5 mM IPTG and 100 μg/ml carbenicillin. Following overnight induction of the plates, the L1 synchronized worms were dropped onto the plates, and worms were harvested at L4 stage for analysis.

Plasmids preparation

C. elegans and human Maf1 3XFlag constructs were taken from a previous study [10]. MAFR-1 and *tm6082* GFP constructs were prepared by PCR amplification using cDNA from N2 WT and *tm6082* strain, respectively. PCR product was cloned into C-terminal GFP

using Topo cloning kit (Invitrogen). The 3XFlag constructs of *tm6082* and ΔC and the different mutations in C-box of human Maf1 were performed using site-directed mutagenesis kit (NEB). GFP constructs of human Maf1 and ΔC constructs were PCR amplified using Flag constructs and inserted in C-terminal GFP using Topo cloning kit. Different mutations in GFP constructs were carried out using site-directed mutagenesis kit.

Cell culture

Human cell lines HEK293T (ATCC) and HepG2 (ATCC) were maintained in Dulbecco's modified Eagle's medium (Invitrogen) supplemented with 10% heat inactivated fetal bovine serum (Gibco) and antibiotic–antimycotic solution (Invitrogen). Cells were grown in a humidified incubator at 37 °C with 5% CO_2. Cells were plated (1×10^5/well) in poly-D-Lysine-coated 6 and 12 well plates (BD Biosciences), and transfections of different constructs or MAF1 Silencer select siRNA (Ambion) were performed using Lipofectamine 3000 (Invitrogen) as described in the manufacturer's instruction. Then, 20–24 h post-transfection, cells were exposed to MMS (Ultra Scientific), rapamycin (Cayman Chemical), MG132 (Sigma), and PD150606 (Tocris Biosciences) for time indicated. All the compounds were prepared in fresh media with 0.1% DMSO (Sigma) as final assay concentration.

Fat staining

L1 synchronized worms were dropped in plates containing either control RNAi or *mafr-1* RNAi OP50 strain. Worms were harvested at L4 stage, and Nile red staining was performed as described previously [10,23]. Image was captured using Zeiss Axio imager microscopes with M2m camera (Zeiss), and fluorescence intensity of individual worms was measured using ImageJ software.

For Oil red O staining, HepG2 cells were plated at density of 1×10^5/well in 12 well plate (BD Biosciences) containing poly-D-lysine (Corning)-coated coverslips. Then, 30 h post-transfection, cells were washed with phosphate buffered saline (Invitrogen) and fixed with 10% neutral buffered formalin [4 g NaH2PO4, 6.5 g Na2HPO4, and 100 ml of 37% formaldehyde in 1 L distilled water (pH 6.8)] for 1 h at RT, followed by two times wash with distilled H_2O. Cells were incubated with 60% Isopropanol for 5 min and then stained with freshly prepared 60% Oil red O solution for 20 min at RT. Cells were washed with H_2O and counterstained with Hematoxylin (Sigma). Cells were imaged on a Zeiss Axio imager microscope with M2m camera (Zeiss). The number of lipid droplets in each cell was quantified using ImageJ software.

Reproduction assays

Egg laying was assessed daily as previously described (Khanna *et al.*) [10]. In short, the WT and *tm6082* L4 stage worms were picked and dropped in 6-cm OP50 plates with one worm per plate. Every day, the worms were transferred onto a new plate, and the progenies were counted. Animals that crawled off the plate were censored for reproductive output from that day forward.

Gene expression

L4 worms and cell lines were lysed in trizol reagent (Zymogen), and RNA extraction was performed using RNA mini prep kit (Zymogen). The DNase treatment was performed as per the kit instruction. The RNA quantity and quality were measured in DS-11 spectrophotometer (DeNovix). Then, 800 ng RNA was used to prepare cDNA using qScript cDNA synthesis kit (Quanta Biosciences). cDNA was diluted, and the quantitative PCR was performed using SYBR Green (BioRad). Primers were described previously [10].

Microarray was performed for L4 stage worms as described previously [10] with three biological replicates for each group. Data analysis was performed using NGS and microarray data analysis software, Partek Genomic Suite (Partek).

Western blot

For whole-cell lysate analysis, cells were lysed in radioimmunoprecipitation assay (RIPA buffer [150 mM NaCl, 1% TritonX-100, 0.5% sodium deoxycholate, 0.1% SDS, and 50 mM Tris (pH 8)] containing protease–phosphatase inhibitor (Thermo Scientific) and PMSF (Sigma). For nuclear–cytoplasmic fractionation, cells were first lysed in cytoplasmic extract buffer containing 10 mM Hepes (Invitrogen), 0.1 mM EDTA (Sigma), 10 mM KCl (Sigma) and 0.3% Igepal (Sigma), protease–phosphatase inhibitor, and PMSF for 20 min on ice. For proper lysis, cells were vortexed for 2–3 s in a 5-min interval, followed by centrifugation at 4 °C. Supernatants containing cytoplasmic fraction were saved, and the pellets were washed with 700 μl cytoplasmic extract buffer (without Igepal) and centrifuged for 10 min at 4 °C. Nuclear pellets were lysed in RIPA buffer containing protease–phosphatase inhibitor and PMSF for 15 min on ice and centrifuged for 15 min at 4 °C to collect the supernatant. Protein quantification was performed using Bradford reagent (Amresco) using SpectraMax spectrophotometer (Molecular devices), and equal amount of protein was resolved in 12% SDS gel (Invitrogen) with 2-(*N*-morpholino)ethanesulfonic acid (MES) sodium dodecyl sulfate (SDS) running buffer (Invitrogen). For detection of phosphorylated proteins, 10% SuperSep phostag gels (Wako) were used with Tris-Glycine SDS running buffer (Invitrogen). Dephosphorylated samples for Phostag gels were prepared by treating the control samples with Lambda protein phosphatase (NEB) for 30 min at 30 °C. Following band separation, proteins were transferred onto nitrocellulose membrane (Amersham Biosciences) and probed with Anti Flag (Sigma), SP1 (Santa Cruz Biotechnology), and β-Actin (Sigma) antibodies. The horseradish peroxidase (HRP)-conjugated anti-mouse and anti-rabbit (Pierce) were used at 1:30,000 and 1:10,000, respectively, for 1 h at RT. The immunoreactive complex was detected by SuperSignal West Pico chemiluminescent substrate (Thermo Scientific) using FluorChem E (Cell Biosciences). The bands were quantified using the ImageJ software (National Institute of Health). For whole-cell lysate and cytoplasmic fractions, β-Actin was used to normalize the band density of the protein of interest, while SP1 was used to normalize nuclear fractions.

Statistical analysis

Statistical significance between two groups was determined using Student's *t*-test and, for multiple group comparison, ANOVA, followed by either Dunnett's or Bonferroni's post-test.

Statistical analyses were performed using the GraphPad Prism 6 software (GraphPad software).

Supplementary Material

Refer to Web version on PubMed Central for supplementary material.

Acknowledgments

We thank L. Thomas and M. He for technical support; J. Lo, D. Lynn, and B. Spatola for critical reading and comments on the manuscript; and the CGC, funded by NIH Office of Research Infrastructure Programs (P40 OD010440), for some strains. We acknowledge support from NIH grants R00AG032308 (S.P.C.) and R01GM109028 (S.P.C.), the American Heart Association (S.P.C.), an Ellison New Scholar Award (S.P.C.), and the American Federation for Aging Research (S.P.C.).

Abbreviations used

pol	polymerase
PKA	protein kinase A
TOR	target of rapamycin
TORC1	TOR complex 1
SREBP	sterol regulatory element binding protein
WT	wild-type
NLS	nuclear localization signal
UPS	ubiquitin proteasome system
MMS	methyl methanesulfonate
aa	amino acid
GO	gene ontology
qRT-PCR	quantitative real time-PCR
GFP	green fluorescence protein
SEM	standard error of the mean
RNAi	RNA interference
MES	2-(*N*-morpholino)ethanesulfonic acid
RIPA	radioimmunoprecipitation assay
SEM	standard error of the mean
RNAi	RNA interference
MES	2-(*N*-morpholino)ethanesulfonic acid

References

1. Bonhoure N, Byrnes A, Moir RD, Hodroj W, Preitner F, Praz V, Marcelin G, Chua SC Jr, Martinez-Lopez N, Singh R, et al. Loss of the RNA polymerase III repressor MAF1 confers obesity resistance. Genes Dev. 2015; 29:934–947. [PubMed: 25934505]
2. Cai Y, Wei YH. Distinct regulation of Maf1 for lifespan extension by protein kinase A and Sch9. Aging (Albany NY). 2015; 7:133–143. [PubMed: 25720796]
3. Cai Y, Wei YH. Stress resistance and lifespan are increased in *C. elegans* but decreased in *S. cerevisiae* by mafr-1/maf1 deletion. Oncotarget. 2016; 7:10,812–10,826.
4. Desai N, Lee J, Upadhya R, Chu Y, Moir RD, Willis IM. Two steps in Maf1-dependent repression of transcription by RNA polymerase III. J Biol Chem. 2005; 280:6455–6462. [PubMed: 15590667]
5. Gajda A, Towpik J, Steuerwald U, Muller CW, Lefebvre O, Boguta M. Full repression of RNA polymerase III transcription requires interaction between two domains of its negative regulator Maf1. J Biol Chem. 2010; 285:35,719–35,727.
6. Johnson SS, Zhang C, Fromm J, Willis IM, Johnson DL. Mammalian Maf1 is a negative regulator of transcription by all three nuclear RNA polymerases. Mol Cell. 2007; 26:367–379. [PubMed: 17499043]
7. Kamath RS, Fraser AG, Dong Y, Poulin G, Durbin R, Gotta M, Kanapin A, Le Bot N, Moreno S, Sohrmann M, et al. Systematic functional analysis of the *Caenorhabditis elegans* genome using RNAi. Nature. 2003; 421:231–237. [PubMed: 12529635]
8. Kantidakis T, Ramsbottom BA, Birch JL, Dowding SN, White RJ. mTOR associates with TFIIIC, is found at tRNA and 5S rRNA genes, and targets their repressor Maf1. Proc Natl Acad Sci U S A. 2010; 107:11,823–11,828. [PubMed: 20018743]
9. Johnson DL, Stiles BL. Maf1, A New PTEN Target Linking RNA and Lipid Metabolism. Trends Endocrinol Metab. 2016 Oct; 27(10):742–750. http://dx.doi.org/10.1016/j.tem.2016.04.016 Review. [PubMed: 27296319]
10. Khanna A, Johnson DL, Curran SP. Physiological roles for mafr-1 in reproduction and lipid homeostasis. Cell Rep. 2014; 9:2180–2191. [PubMed: 25497095]
11. Khanna A, Pradhan A, Curran SP. Emerging roles for Maf1 beyond the regulation of RNA polymerase III activity. J Mol Biol. 2015; 427:2577–2585. [PubMed: 26173035]
12. Kimble J, Sharrock WJ. Tissue-specific synthesis of yolk proteins in *Caenorhabditis elegans*. Dev Biol. 1983; 96:189–196. [PubMed: 6825952]
13. Li Y, Kwan Tsang C, Wang S, Li X, Yang Y, Fu L, Huang W, Li M, Wang HY, Steven Zheng XF. MAF1 suppresses AKT–mTOR signaling and liver cancer through activation of PTEN transcription. Hepatology. 2016; 63:1928–1942. http://dx.doi.org/10.1002/hep.28507. [PubMed: 26910647]
14. Lynn DA, Dalton HM, Sowa JN, Wang MC, Soukas AA, Curran SP. Omega-3 and -6 fatty acids allocate somatic and germline lipids to ensure fitness during nutrient and oxidative stress in *Caenorhabditis elegans*. Proc Natl Acad Sci U S A. 2015; 112:15,378–15,383.
15. Melo JA, Ruvkun G. Inactivation of conserved *C. elegans* genes engages pathogen- and xenobiotic-associated defenses. Cell. 2012; 149:452–466. [PubMed: 22500807]
16. Michels AA, Robitaille AM, Buczynski-Ruchonnet D, Hodroj W, Reina JH, Hall MN, Hernandez N. mTORC1 directly phosphorylates and regulates human MAF1. Mol Cell Biol. 2010; 30:3749–3757. [PubMed: 20516213]
17. Michels AA. MAF1: a new target of mTORC1. Biochem Soc Trans. 2011 Apr; 39(2):487–491. http://dx.doi.org/10.1042/BST0390487 Review. [PubMed: 21428925]
18. Mierzejewska J, Chreptowicz K. Lack of Maf1 enhances pyruvate kinase activity and fermentative metabolism while influencing lipid homeostasis in *Saccharomyces cerevisiae*. FEBS Lett. 2016; 590:93–100. [PubMed: 26787463]
19. Moir RD, Lee J, Haeusler RA, Desai N, Engelke DR, Willis IM. Protein kinase A regulates RNA polymerase III transcription through the nuclear localization of Maf1. Proc Natl Acad Sci U S A. 2006; 103:15,044–15,049. [PubMed: 16373501]
20. Oficjalska-Pham D, Harismendy O, Smagowicz WJ, Gonzalez de Peredo A, Boguta M, Sentenac A, Lefebvre O. General repression of RNA polymerase III transcription is triggered by protein

phosphatase type 2A-mediated dephosphorylation of Maf1. Mol Cell. 2006; 22:623–632. [PubMed: 16762835]

21. Orioli A, Praz V, Lhôte P, Hernandez N. Human MAF1 targets and represses active RNA polymerase III genes by preventing recruitment rather than inducing long-term transcriptional arrest. Genome Res. 2016; 26:624–635. [PubMed: 26941251]
22. Palian BM, Rohira AD, Johnson SA, He L, Zheng N, Dubeau L, Stiles BL, Johnson DL. Maf1 is a novel target of PTEN and PI3K signaling that negatively regulates oncogenesis and lipid metabolism. PLoS Genet. 2014; 10:e1004789. [PubMed: 25502566]
23. Pino EC, Webster CM, Carr CE, Soukas AA. Biochemical and high throughput microscopic assessment of fat mass in *Caenorhabditis elegans*. J Vis Exp. 2013; 30(73) http://dx.doi.org/10.3791/50180.
24. Reina JH, Azzouz TN, Hernandez N. Maf1, a new player in the regulation of human RNA polymerase III transcription. PLoS One. 2006; 1:e134. [PubMed: 17205138]
25. Rideout EJ, Marshall L, Grewal SS. Drosophila RNA polymerase III repressor Maf1 controls body size and developmental timing by modulating tRNAiMet synthesis and systemic insulin signaling. Proc Natl Acad Sci U S A. 2012; 109:1139–1144. [PubMed: 22228302]
26. Roberts DN, Wilson B, Huff JT, Stewart AJ, Cairns BR. Dephosphorylation and genome-wide association of Maf1 with Pol III-transcribed genes during repression. Mol Cell. 2006; 22:633–644. [PubMed: 16762836]
27. Rohira AD, Chen CY, Allen JR, Johnson DL. Covalent small ubiquitin-like modifier (SUMO) modification of Maf1 protein controls RNA polymerase III-dependent transcription repression. J Biol Chem. 2013; 288:19,288–19,295.
28. Lee YL, Li YC, Su CH, Chiao CH, Lin IH, Hsu MT. MAF1 represses CDKN1A through a Pol III-dependent mechanism. Elife. 2015; 4:e06283. http://dx.doi.org/10.7554/eLife.06283. [PubMed: 26067234]
29. Rollins J, Veras I, Cabarcas S, Willis I, Schramm L. Human Maf1 negatively regulates RNA polymerase III transcription *via* the TFIIB family members Brf1 and Brf2. Int J Biol Sci. 2007; 3:292–302. [PubMed: 17505538]
30. Rossi KA, Weigelt CA, Nayeem A, Krystek SR Jr. Loopholes and missing links in protein modeling. Protein Sci. 2007; 16:1999–2012. [PubMed: 17660258]
31. Shibata Y, Branicky R, Landaverde IO, Hekimi S. Redox regulation of germline and vulval development in *Caenorhabditis elegans*. Science. 2003; 302:1779–1782. [PubMed: 14657502]
32. Shor B, Wu J, Shakey Q, Toral-Barza L, Shi C, Follettie M, Yu K. Requirement of the mTOR kinase for the regulation of Maf1 phosphorylation and control of RNA polymerase III-dependent transcription in cancer cells. J Biol Chem. 2010; 285:15,380–15,392.
33. Boguta M. a. general negative regulator of R.N.A. polymerase I.I.I. in yeast Maf1. Biochim Biophys Acta. 2013 Mar-Apr;1829(3–4):376–384. http://dx.doi.org/10.1016/j.bbagrm.2012.11.004 Review. [PubMed: 23201230]
34. Tao T, Shi H, Guan Y, Huang D, Chen Y, Lane DP, Chen J, Peng J. Def defines a conserved nucleolar pathway that leads p53 to proteasome-independent degradation. Cell Res. 2013; 23:620–634. [PubMed: 23357851]
35. Upadhya R, Lee J, Willis IM. Maf1 is an essential mediator of diverse signals that repress RNA polymerase III transcription. Mol Cell. 2002; 10:1489–1494. [PubMed: 12504022]
36. Walker AK, Jacobs RL, Watts JL, Rottiers V, Jiang K, Finnegan DM, Shioda T, Hansen M, Yang F, Niebergall LJ, et al. A conserved SREBP-1/phosphatidylcholine feedback circuit regulates lipogenesis in metazoans. Cell. 2011; 147:840–852. [PubMed: 22035958]
37. Warner JR. The economics of ribosome biosynthesis in yeast. Trends Biochem Sci. 1999; 24:437–440. [PubMed: 10542411]
38. Wei Y, Tsang CK, Zheng XF. Mechanisms of regulation of RNA polymerase III-dependent transcription by TORC1. EMBO J. 2009; 28:2220–2230. [PubMed: 19574957]
39. Wei Y, Zheng XS. Maf1 regulation: a model of signal transduction inside the nucleus. Nucleus. 2010; 1:162–165. [PubMed: 21326948]
40. Willis IM, Desai N, Upadhya R. Signaling repression of transcription by RNA polymerase III in yeast. Prog Nucleic Acid Res Mol Biol. 2004; 77:323–353. [PubMed: 15196897]

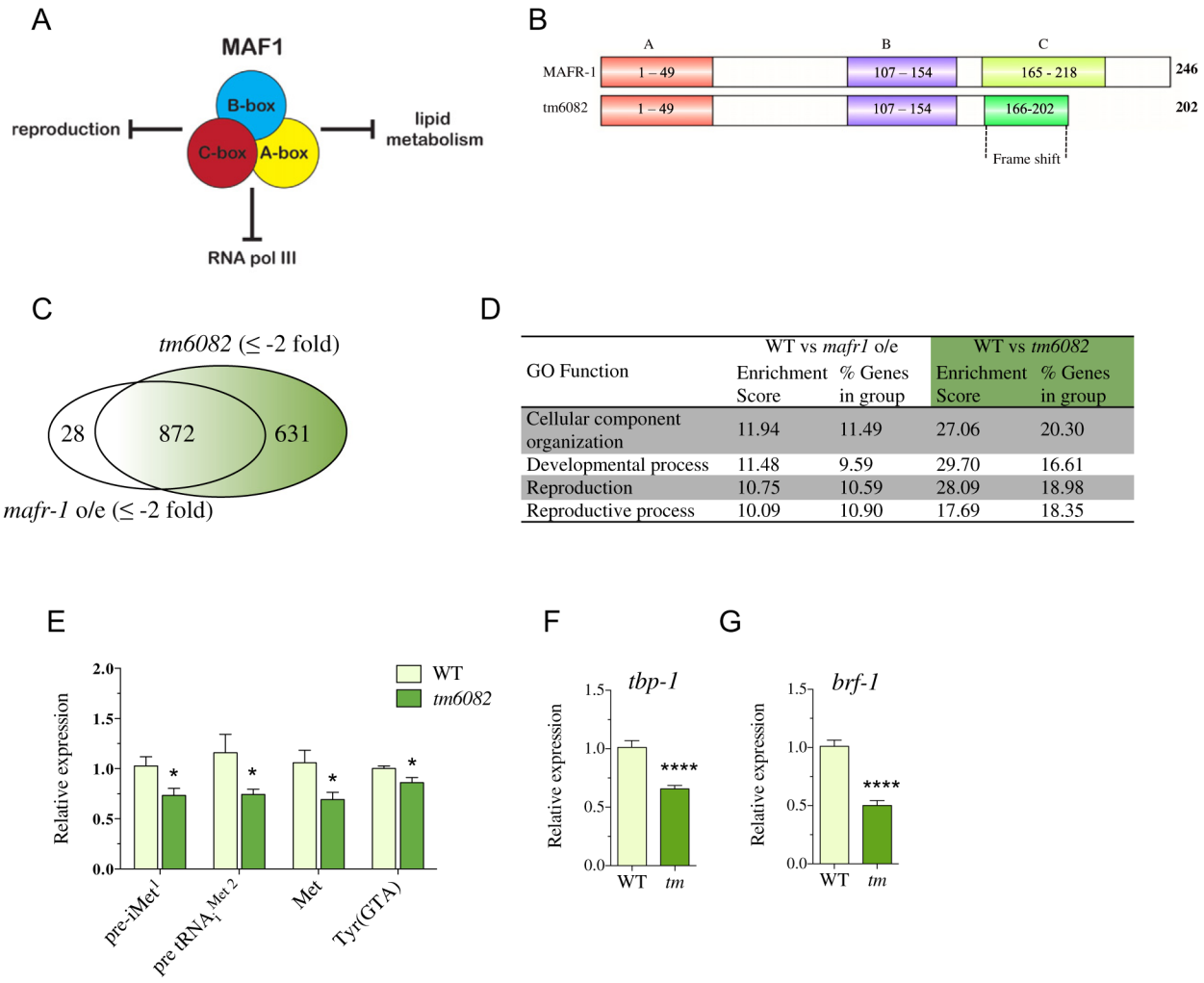

GO Function	WT vs *mafr1* o/e		WT vs *tm6082*	
	Enrichment Score	% Genes in group	Enrichment Score	% Genes in group
Cellular component organization	11.94	11.49	27.06	20.30
Developmental process	11.48	9.59	29.70	16.61
Reproduction	10.75	10.59	28.09	18.98
Reproductive process	10.09	10.90	17.69	18.35

Fig. 1.

Deletion of C-box renders MAFR-1 hyperactivated. (A) Schematic of the cellular phenotypes influenced by Maf1. (B) Cartoon representation of the MAFR-1 regions in the *mafr-1(tm6082)* mutant. (C) Venn diagram of the microarray transcriptional profiling of *mafr-1o/e* and *mafr-1(tm6082)* mutant as compared to WT. Out of 900 and 1503 genes downregulated in *mafr-1o/e* and *tm6082*, respectively, 872 genes were common for both, while 28 and 631 genes were unique for *mafr-1o/e* and *tm6082*, respectively. (D) Microarray analysis of downregulated genes with respect to WT with a fold change of ±2 and FDR of ≤0.01 was considered significant. Fischer's exact test was used to calculate GO enrichment score. Enrichment $p<0.001$. (E–G) qRT-PCR expression analysis of MAFR-1-dependent (E) RNA pol III and (F and G) RNA pol II target genes was performed for L4 stage WT and *tm6082* mutant animals (abbreviated tm). Data represent mean ± SEM from eight independent samples. Student's *t*-test, * $p < 0.05$, **** $p < 0.001$.

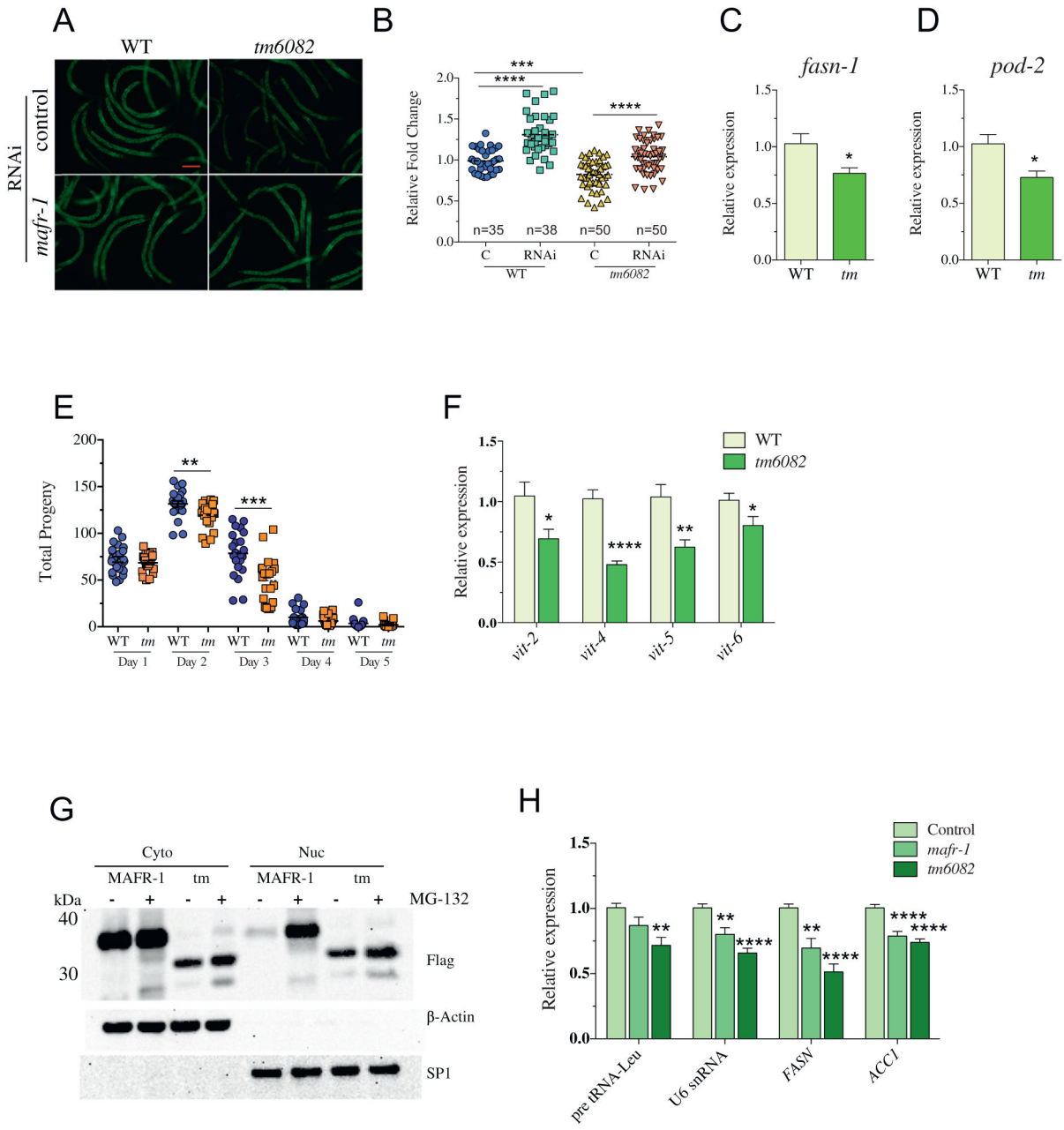

Fig. 2.

MAFR-1gf is nuclear and represses lipid biogenesis and reproduction. (A and B) The (A) fluorescent imaging of Nile red-stained stored lipids in L4 stage WT and *mafr-1(tm6082)* (abbreviated tm) animals grown on OP50 control RNAi and *mafr1* RNAi and the (B) subsequent quantification using ImageJ software. Data represent mean ± SEM from indicated number (*n*) of animals measured. ANOVA test followed by Bonferroni's post-test, *** p <0.001, **** p < 0.001. (C and D) Expression of lipid biogenesis genes (C) *fasn-1* and (D) *pod-2/ACC* for L4 stage worms. Data represent mean ± SEM from eight independent samples. Student's *t*-test, * p < 0.05. (E) Reproductive output in WT and *mafr-1(tm6082)* animals. Data represent mean ± SEM from 24 animals. Student's *t*-test, **

$p < 0.01$, *** $p < 0.001$. (F) qRT-PCR expression analysis of vitellogenin genes in WT and *mafr-1(tm6082)* animals. Data represent mean ± SEM from eight independent samples. Student's *t*-test, * $p < 0.05$, ** $p < 0.01$, **** $p < 0.001$. (G) Western blot analysis of nuclear and cytoplasmic fractionation following overexpression in HEK293T cells and 5-h treatment with either DMSO (Control) or 10 3M MG132. (H) qRT-PCR expression analysis of human RNA pol III (pre tRNA-Leu and U6 snRNA) and RNA pol II (*FASN* and *ACC1*) in HEK293T cells following transfection with MAFR-1 and MAFR-1(tm6082) 3XFlag-tagged constructs. Data represent mean ± SEM from three independent experiments, $n = 12$. ANOVA test followed Dunnett's post-test *$p < 0.05$, **$p < 0.01$, **** $p < 0.001$.

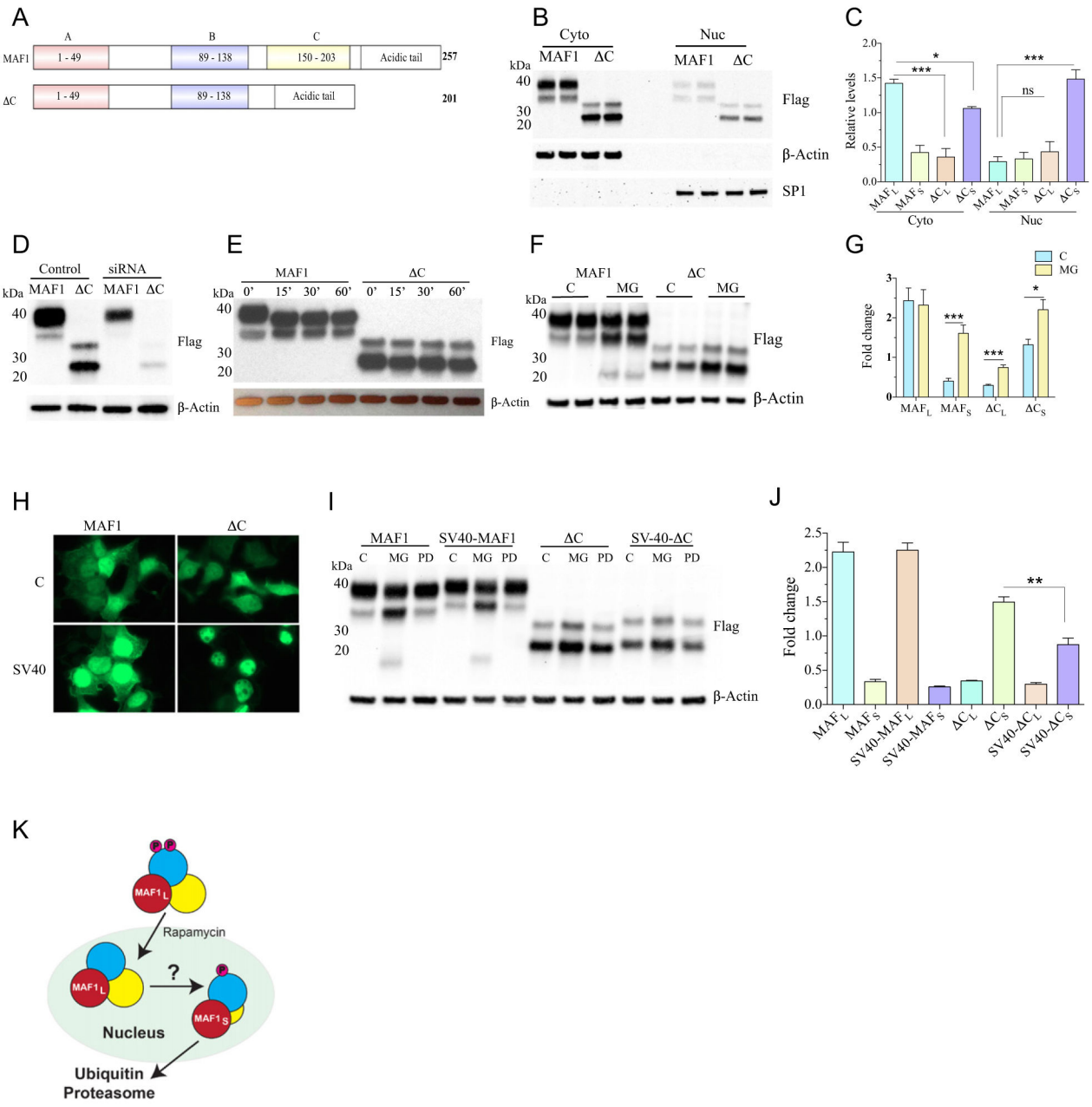

Fig. 3.

Human MAF1 protein turnover is proteasome mediated and occurs in the nucleus. (A) Cartoon representation of human MAF1 and deletion of 56 aa from C-box region in ΔC. (B and C) Cytoplasmic and nuclear fractions of HEK293T cells expressing MAF1 and ΔC; (B) two biological replicates shown and quantification of $MAF1_L$ and $MAF1_S$ in WT, and ΔC_S species. β-Actin was used to normalize the band intensity of cytoplasmic MAF1, while SP1 for nuclear MAF1. (C) quantification of $MAF1_L$ and $MAF1_S$ in WT and ΔC_S and ΔC_L species. β-Actin was used to normalize the band intensity of cytoplasmic fractions, while SP1 for nuclear fractions. $MAF1_L$ level was compared to ΔC_L and ΔC_S for both cytoplasmic and nuclear fractions using one-way ANOVA followed by Dunnett's post-test. Mean ± SEM,

$n = 3$. * $p < 0.05$, *** $p < 0.001$. (D) siRNA of MAF1 depletes both $MAF1_L$ and $MAF1_S$ in HEK-293T cells. (E) Western blot analysis of MAF1 and ΔC following phosphatase treatment for 0, 15, 30, and 60 min. (F and G) Overexpression in HEK-293T cells followed by MG132 treatment (10 μM) for 3 h affects $MAF1_S$, ΔCL, and ΔC_S abundance; (F) two biological replicates shown and quantified in (G). Data represent mean ± SEM from five independent experiments. Student's *t*-test, * $p < 0.05$, *** $p < 0.001$. MG = MG132 treated, C = DMSO control. (H and I) The (H) GFP imaging of MAF1 and ΔC with and without SV40-NLS sequences, (I) which drives protein turnover in a proteasome- but not calpain-dependent manner. (J) Quantification of large and small bands from control samples using ImageJ software. Statistical significance was performed to analyze if the inclusion of SV-40 NLS can change the expression of MAF1 and ΔC large and small bands. Data represent mean ± SEM from three independent experiments. Student's *t*-test, ** $p < 0.01$. MG = MG-132 treated, PD = PD150606 treated, C = DMSO control. (K) Cartoon representation of nuclear MAF1 turnover.

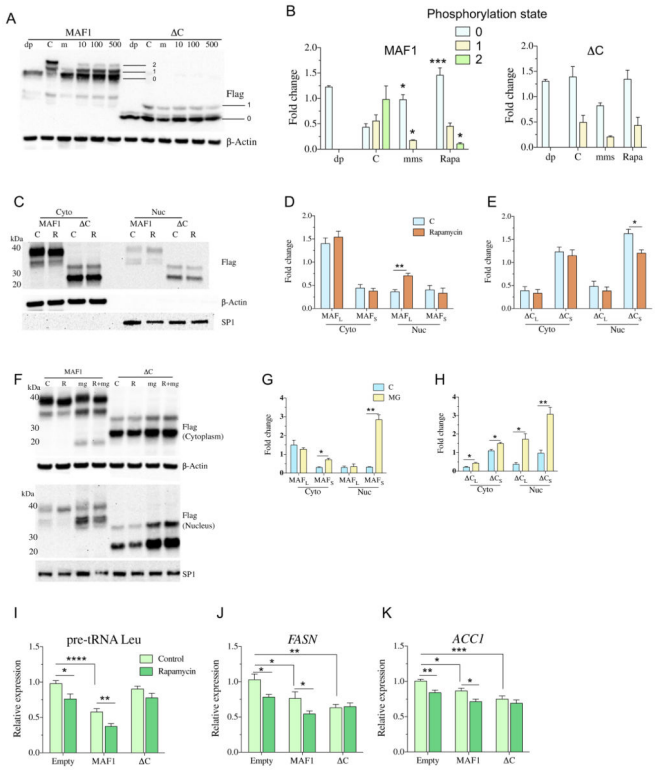

Fig. 4.

C-box regulates rapamycin response and stability of $MAF1_L$. (A and B) Western blot of Phos-tag® gel showing phosphorylated and dephosphorylated bands following treatment with (C) DMSO, 0.03% MMS (m), and 10, 100, and 500 nM of rapamycin for 3 h in HEK293T cells. For dephosphorylated band analysis, untreated cells were lysed, and phosphatase treatment was performed for 30 min (dp). Bands were quantified in (B), where each treated band is normalized to β-Actin levels. The numbers indicate 0 = smallest band, 1 = middle band, and 2 = topmost band. Data represent mean ± SEM from three independent experiments. Student's *t*-test was performed for each band in the treated group to their respective band in the control group, * $p < 0.05$, *** $p < 0.001$. dp = phosphatase treated, m = 0.03% MMS, 10 = 10 nM rapamycin, 100 = 100 nM rapamycin, 500 = 500 nM rapamycin, C = DMSO control. (C–E) Western blot of MAF1 and ΔC cytoplasmic and nuclear fractions after (C) 3 h of treatment with 10 nM rapamycin in HEK293T cells, and (D) quantification of $MAF1_L$ and $MAF1_S$ and (E) ΔC_L and ΔC_S bands using β-Actin as a normalizing control for cytoplasmic fractions while SP1 for nuclear fractions. Data represent mean ± SEM from four independent experiments. Student's *t*-test, * $p < 0.05$, ** $p < 0.01$. R = 10 nM rapamycin, C = DMSO control. (F–H) Western blot of MAF1 and ΔC cytoplasmic and nuclear fractions following (F) 3 h of treatment with 10 nM rapamycin and 10 μM MG-132 in HEK293T cells and quantified for (G) $MAF1_L$ and $MAF1_S$ and (H) ΔC_L and ΔC_S. Data represent mean ± SEM from three independent experiments. Student's *t*-test, * $p < 0.05$, ** $p < 0.01$. R = 10 nM rapamycin, mg = 10 μM MG132, R + mg = 10 nM rapamycin and 10 μM MG-132 treatment, C = DMSO control. (I–K) qPCR analysis of pol III and pol II targets following 6-h exposure of 10 nM rapamycin in HEK-293T cells. Data represent mean ± SEM from three independent experiments, $n = 12$. Student's *t*-test was

performed to determine statistical significance between the control and the respective rapamycin-treated group, while ANOVA followed by Dunnett's post-test was used for multivariable analysis.

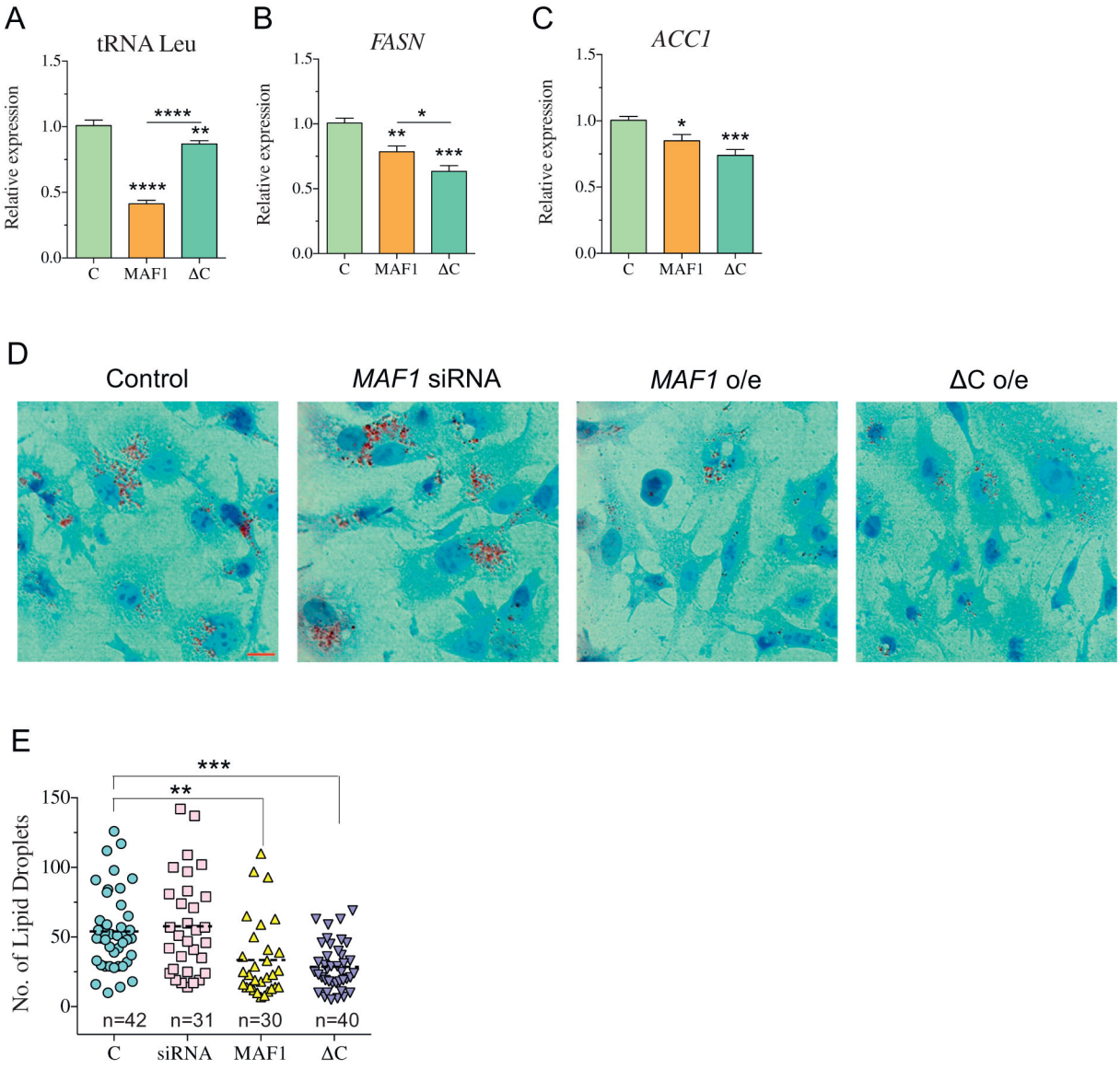

Fig. 5.

MAF1 and ΔC negatively regulate lipid biogenesis in HepG2 cells. (A–C) Expression of (A) pre-tRNA Leu, (B) *FASN,* and (C) *ACC1* following 24 h post-transfection. Data represent mean ± SEM from three independent experiments, $n = 12$. ANOVA followed by Dunnett's test was used to compare MAF1 and ΔC with respect to the control group, while Student's *t*-test was used to compare the difference between MAF1 and ΔC, * $p < 0.05$, ** $p < 0.01$, *** $p < 0.001$, **** $p < 0.001$. (D) Oil red O staining 30 h post-transfection. (E) Quantification of lipid droplets using Image J software. Each data point represents lipid droplets from a single cell. Data represent mean ± SEM from indicated number (*n*) of cells quantified. ANOVA test followed by Dunnett's post-test, * $p < 0.05$, ** $p < 0.01$.

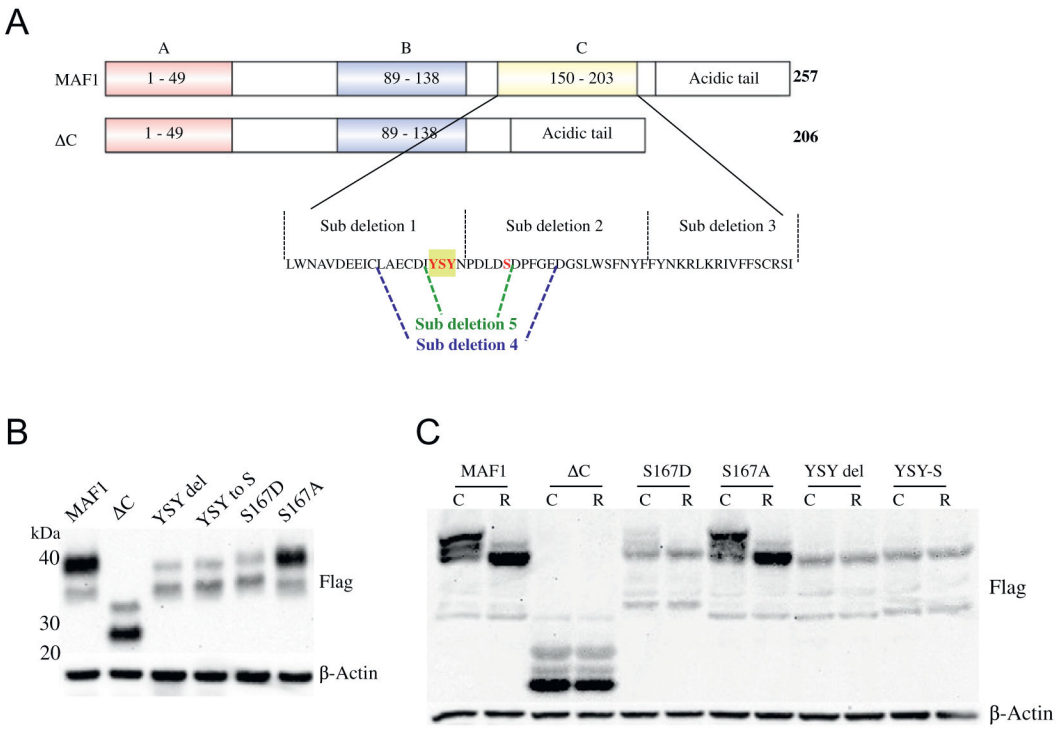

Fig. 6.

YSY motif in the C-box region regulates MAF1 stability. (A) Cartoon representation of deletions and substitutions used to narrow down rapamycin-responsive residues in the C-box; residues in red were modified as indicated. (B) Western blot analysis of YSY mutants generated. (C) Phostag gel of MAF1 mutants following exposure to 10 nM rapamycin for 3 h. R = rapamycin treatment, C = DMSO control.

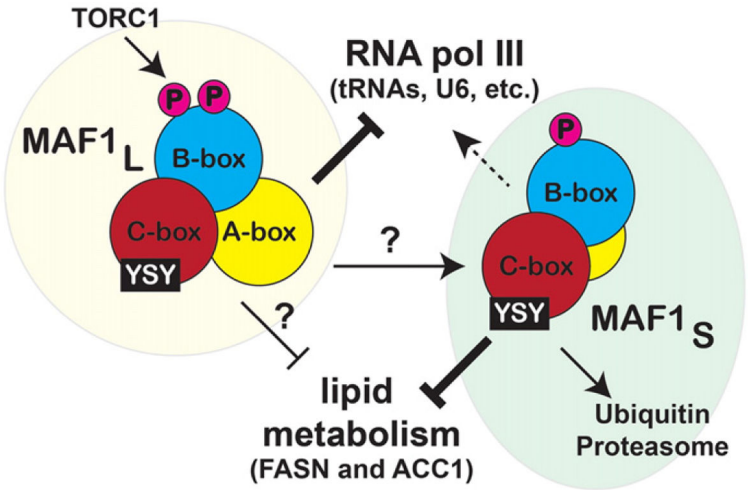

Fig. 7.

Integrated model of MAF1 function and regulation. Cartoon depiction of the differential regulation and activities of the $MAF1_L$ and $MAF1_S$ species. Our model also shows that $MAF1_s$ is readily targeted by UPS, and YSY seems to be an important motif that regulates MAF1 stability and function.